

## Protocols for Harmonized Quantification and Noise Reduction in Low Dose Oncological 18F-FDG PET/CT Imaging

Marcos A. D. Machado<sup>1,2</sup>

Vinícius O. Menezes<sup>1,3</sup>

Mauro Namías<sup>4</sup>

Naiara S. Vieira<sup>1</sup>

Cleiton C. Queiroz<sup>1,5</sup>

Roberta Matheoud<sup>6</sup>

Adam M. Alessio<sup>7</sup>

Mércia L. Oliveira<sup>8</sup>

*<sup>1</sup>Nuclear Medicine Department, São Rafael Hospital, Brazil*

*<sup>2</sup>Hospital das Clínicas da Universidade Federal de Bahia/Ebserh, Brazil*

*<sup>3</sup>Hospital das Clínicas da Universidade Federal de Pernambuco/Ebserh, Brazil*

*<sup>4</sup>Fundación Centro Diagnóstico Nuclear, Argentina*

*<sup>5</sup>Hospital Universitario Professor Alberto Antunes/Ebserh, Brazil*

*<sup>6</sup>Department of Medical Physics, Azienda Ospedaliera Maggiore della Carità, Italy*

*<sup>7</sup>Department of Radiology, University of Washington, USA*

*<sup>8</sup>Centro Regional de Ciências Nucleares (CRCN – NE)/ CNEN, Brazil*

Correspondence to: Marcos Machado, Nuclear Medicine Department, Hospital São Rafael, Avenida São Rafael, 2152 - São Marcos, Salvador - BA, 41253-190, Brazil. Tel. +55 71 3281-6891. Fax. +55 71 3281-6327. E-mail: [machado@radtec.com.br](mailto:machado@radtec.com.br)

Word count: 5897

**Running title: Harmonized Low Dose Oncological PET**

## ABSTRACT

**Purpose:** Oncological 18F-FDG PET/CT acquisition and reconstruction protocols need to be optimized for both quantitative and detection tasks. To date, most studies have focused on either quantification or noise, leading to quantitative harmonization guidelines or appropriate noise levels. We developed and evaluated protocols that provide harmonized quantitation with optimal amount of noise as a function of acquisition parameters and body mass. **Methods:** Multiple image acquisitions (N=17) of the IEC/NEMA PET image quality phantom were performed with variable counting statistics. Phantom images were reconstructed with OSEM3D and PSF reconstructions for harmonized  $CRC_{max}$  quantification. The lowest counting statistics that resulted in compliance with EANM recommendations for  $CRC_{max}$  and  $CRC_{max}$  variability were used as optimization metrics. Image noise in the liver of 48 typical oncological 18F-FDG PET/CT studies was analysed with OSEM3D and PSF harmonized reconstructions. 164 additional 18F-FDG PET/CT reconstructed list mode images were also evaluated to derive analytical expressions that predict image quality and noise variability. Phantom to subject translational analysis was used to derive optimized acquisition and reconstruction protocols. **Results:** For harmonized quantitation levels, PSF reconstructions yielded decreased noise and lower  $CRC_{max}$  variability compared with regular OSEM3D reconstructions, suggesting they could enable a decreased activity regimen for matched performance. **Conclusion:** A PSF reconstruction with 7mm post-filter can provide harmonized quantification performance and acceptable image noise levels with injected activity, duration, and mass settings of 260 MBq.s/kg acquisition parameter at scan time. Similarly, the OSEM3D with 5mm post filter can provide similar performance with 401 MBq.s/kg.

Key words: PET/CT protocols; optimization; quantification; biomarker; EARL accreditation

## INTRODUCTION

Positron emission tomography (PET) and computed tomography (CT) hybrid imaging (PET/CT) using 18F-fluorodeoxyglucose (18F-FDG) is an important tool in the management of oncological patients for clinical diagnosis, staging, prognosis and treatment response assessment (1-3). Optimal PET/CT imaging should result in consistent diagnostic image quality and quantification with minimal costs and radiation exposure. The use of PET as a quantitative imaging biomarker requires standardization and harmonization of imaging procedures to obtain reproducible quantitative metrics. PET/CT acquisition and reconstruction protocols optimized to meet international quantitative standards might not necessarily be optimized for lesion detection tasks (4,5). The introduction of point spread function (PSF) modeling in reconstruction algorithms has shown to increase detection performance of small and low-intensity lesions (6,7,8,9), but standardized uptake value (SUV) quantification of small lesions has lower reproducibility due to increased ensemble noise when low gaussian filters (optimized for detection) are used (10,11).

During the last few years, several facilities have adopted the European Association of Nuclear Medicine (EANM) guidelines through the EANM Research Ltd. (EARL) FDG-PET/CT accreditation program (12) as a standard for PET SUV quantification (12,13, 14). Despite the wide literature regarding the optimization of PET protocols for lesion detectability (6-9,15) or for the impact of noise on quantitation (16-19), there is still limited work optimizing low dose PET as a quantitative biomarker using guidelines such as the EANM criteria (20,21). Advances in PET image reconstruction algorithms that incorporate PSF modeling have reduced noise and increased resolution, potentially allowing for reduced injected activity and thus lower radiation exposure to patients (15,22-25), opening new scenarios for cancer screening with PET (15,26,27).

PET imaging performance is dependent on the scanner model (6-9), acquisition parameters (administered activity and acquisition duration), image reconstruction, and patient

habitus (22-25). The authors have previously suggested acquisition parameter optimization for a particular scanner based on a quadratic or power dose scheme to maintain image noise at a consistent level throughout the population (21,23-25). Image noise is indeed a source of variance in the SUV quantification of tumor and ideally should be maintained constant over the patient population to assure consistent quantification variability (16-19). In general, the reconstruction settings define whether the contrast recovery coefficients (CRCs) are within the harmonization criteria (20). Lasnon *et al* (2013) demonstrated that PSF reconstruction can result in images in quantitative compliance with the EANM guidelines by using additional gaussian filtering (28). However, this approach requires that the detection and quantitative tasks be performed on two different image volumes. Thus, a commercial solution (EQ.PET, Siemens Healthcare) allowing all-in-one diagnostic and quantitative images was validated by Quak *et al*, demonstrating that PSF modeling could be used to provide higher detectability and the EANM quantitative recommendations at the same time (29, 30). Our initiative is also in line with the increasing interest for task-specific protocols, which can reduce costs and increase diagnostic accuracy (26).

The present study aims at developing optimized imaging protocols providing recommendations on acquisition and reconstruction settings to obtain lower injected activities and harmonized quantification according to the EANM guidelines. The EARL procedure specifies that image noise should not exceed 15% and that recovery coefficients should remain unbiased (21). To account for differences on the noise behaviour between standard 3D ordered subset expectation maximization (OSEM3D) and PSF reconstructions, we extended the concept of harmonisation by defining optimal quantification variability levels, which is affected by image noise. Therefore, this work aimed to:

- characterize noise properties of PSF reconstructions,
- verify consistency of a newly defined harmonisation bias index (*HBI*) across acquisition parameters for both OSEM3D and PSF reconstructions, and

- define reconstruction-specific formulas for optimal acquisition parameters that satisfies *HBI*, noise levels and quantification variability.

This work provides a feasible methodology that might be applied in PET centers to decrease the injected activity while achieving consistent image quality and quantification when using PSF reconstructions.

## **MATERIALS AND METHODS**

### **Scanner**

PET/CT imaging was performed on a PET Siemens Biograph TruePoint TrueV (Knoxville, TN, USA) combined with a 16-slice CT scanner (Emotion 16; Siemens). PET images were corrected for random coincidences, normalization, dead time losses, scatter and attenuation. The attenuation map was obtained by a spiral CT scan (100 kVp, automatic tube-current modulation), on a 168x168 matrix size (4.07 x 4.07x 3 mm<sup>3</sup> voxels) and a standard soft tissue reconstruction kernel (Siemens B30s) for both phantom and patients. All images were acquired within 3 months from the cross-calibration between PET scanner and dose calibrator.

### **Phantom study**

#### **Phantom preparation and imaging**

We used a IEC/NEMA body phantom with 6 spheres (internal diameters of 10, 13, 17, 22, 28 and 37 mm) filled with a 18F-FDG stock solution of 45 MBq diluted in 1000 ml and the phantom compartment filled with 42 MBq of 18F-FDG to yield a sphere to background concentration ratio of 10:1, according to the EANM guideline (20). Thereafter we define the phantom activity as the 18F-FDG activity in the background. The *CRC* of the maximum pixel value (*CRC<sub>max</sub>*) is defined as the ratio between the measured activity concentration in the maximum pixel and the actual activity concentration in the sphere. Thus, *CRC<sub>max</sub>* represents the fraction of *SUV<sub>max</sub>* recovery of a given lesion size in patient scans.

Four different cumulated counting levels (Groups A-D) were acquired with multiple acquisitions to evaluate the variance of  $CRC_{max}$ . Sets of PET/CT images were sequentially acquired with two bed positions. The phantom activity and the image duration were adjusted to reproduce equivalent counting within groups as follows:

Group A) 1272 MBq.s/kg, high count

(2 frames @ 26.7 and 23.4 MBq for 449 and 510 s each)

Group B) 416 MBq.s/kg, clinical standard

(5 frames @ 20.0, 19.5, 18.3 and 16.5 MBq for 190, 202, 220, 225 and 235 s each)

Group C) 216 MBq.s/kg

(5 frames @ 12.6, 12.2, 11.7, 11.2 and 10.7 MBq for 160, 165, 170, 180 and 200 s each)

Group D) 81 MBq.s/kg

(5 frames @ 14.3, 14.1, 13.9, 13.7 and 13.5 MBq for 76, 80, 81, 83 and 86 s each)

Acquisition parameters in the phantom - defined as the product between the phantom activity at acquisition time (in MBq) and the acquisition duration per bed position (in seconds) - were normalized by 9.4 kg which is the phantom weight in the background.

## **Reconstruction**

Images were reconstructed with the following algorithms:

- OSEM3D: Ordered-Subsets Expectation Maximization with 3 iterations, 21 subsets and a 5 mm Gaussian filter (EARL harmonized);
- PSF7: Point Spread Function Ordinary Poisson with 3 iterations, 21 subsets and a 7 mm Gaussian filter (EARL harmonized);
- PSF2: Point Spread Function Ordinary Poisson with 2 iterations, 21 subsets and a 2 mm Gaussian filter.
- In addition, the PSF+2mm filter had additional filtering applied with the EQ.PET package (PSF2-EQ\*), where the symbol (\*) denotes the amplitude of gaussian filtering.

The OSEM3D reconstruction is our current clinical standard reconstruction and the PSF2 is used for detection optimization (9,24). All Gaussian filters were 3D isotropic.

### Phantom Image analysis

The  $CRC_{max}$  of the hot spheres were calculated by using an automatic routine provided by the EANM upon request (31), except the PSF2 images which were analyzed with EQ.PET (Siemens, Oxford, UK), by applying varying post filter (6 mm, 6.5 mm and 7 mm) to determine the configuration that complies with the EANM quantification standards.

The protocol was considered harmonized according to EARL standards if the mean value of  $CRC_{max}$  were within the EARL limits. To this extent, we defined an overall harmonization bias index ( $HBI$ ) to measure, for each acquisition and reconstruction protocol, the deviation of  $CRC_{max}$  of each sphere from the corresponding EARL limits:

$$HBI = \frac{1}{6} * \sum_{i=1}^6 \frac{|C_i - L_i| + |C_i - U_i|}{K_i} \text{ (equation 1)}$$

where  $i = 1$  to 6 indicates each phantom sphere,  $C_i$  is the average of  $CRC_{max}$  for sphere “ $i$ ” obtained through repeated acquisitions,  $U_i$  and  $L_i$  are the upper and lower EARL limits for sphere “ $i$ ”, and  $K_i$  is a normalization index calculated as the difference between  $U_i$  and  $L_i$  limits for sphere “ $i$ ”. According to this definition, one expects  $HBI = 1.00$  if the protocol is EARL compliant, and the higher  $HBI$ , the more is the bias from EARL limits.

The of the  $CRC_{max}$  values and mean of the coefficient of variation across spheres were averaged for each group of acquisition and the standard deviation was calculated to estimate the quantification variability of a protocol as follows:

$$Q_{var} = \frac{1}{6} * \sum_{i=1}^6 \left( \frac{\sigma_i}{C_i} \right) \text{ (equation 2)}$$

Where  $\sigma_i$  is the standard deviation of  $CRC_{max}$  across realizations for sphere  $i$ .

Additionally, according to PERCIST criteria 1.0 (32) we defined a spherical volume of interest (VOI) of 3 cm diameter in the background (Figure 1) to compute the background noise metric coefficient of variation (CV) defined as

$$CV = \frac{\sigma_b}{\mu_b} \text{ (equation 3).}$$

where  $\sigma_b$  and  $\mu_b$  are the standard deviation and the mean pixel value in the VOI, respectively.

### **Patient imaging**

Conventional 18F-FDG-PET patient exams for whole body oncologic workup were randomly selected and excluded based on the following criteria: pregnancy or nursing, motor difficulties, liver metastases, hyperglycemia at the time of tracer administration, or a delay exceeding 90 min between 18F-FDG injection and image acquisition. The study was approved by the Monte Tabor - Hospital São Rafael ethical board and all subjects signed a written informed consent. The images were acquired according to the clinical protocol of Hospital São Rafael for tumor PET imaging. Subjects fasted for 6 hours prior to the 18F-FDG injection.

### **Prospective patient imaging (step 1)**

A total of 48 18F-FDG-PET/CT whole body adult studies (mean body mass:  $69 \pm 15$  kg, range: 36-102 kg) were gathered over a 2-month period and prospectively evaluated. Images were acquired from the mid-thigh to the vertex of the skull of subjects in supine position with the arms positioned above the head. PET scans started  $67 \pm 10$  min (range, 51-90 min) after injection of  $3.1 \pm 0.7$  MBq/kg (range, 1.4-5.8 MBq/kg) and the acquisition duration was adjusted according to the methodology of reference (24) for a given patient weight and injected activity, with  $201 \pm 43$  s (range, 111-300 s).

### **Retrospective list mode imaging (step 2)**

This step aimed at characterizing the noise levels of PSF7 as a function of acquisition parameters. To this extent, we extracted 41 list-mode images of the liver region from database of our previous work (24). Subjects were  $70 \pm 16$  kg (range: 45-120 kg) and injected activity  $3.5 \pm 0.6$  MBq/kg (range: 2.3-4.6 MBq/kg). All 41 list-mode images were acquired for 360 s and



reconstructed at incremental 1 min intervals up to 4 min (4 images per patient) with PSF7 reconstruction, resulting in 164 images.

### **Patient Image analysis**

All images were analyzed with Syngo.VIA version VA30 (Siemens Healthcare). The *CV* was measured in the liver of normal subjects with the same size VOI used for the phantom experiments.

For step 1, OSEM3D and PSF7 were used to analyse the differences in *CV*. Since we aimed at comparing the noise characteristics between both harmonized reconstructions (similar spatial resolution), PSF2 algorithm was not evaluated and may be assessed elsewhere (24).

For step 2, *CV* was analysed through a first-order approximation for the *CV* from the total collected counts as (24):

$$CV = a * (CD)^b \text{ (equation 4).}$$

where *a* and *b* are the regression coefficients, *CD* is the acquisition parameter in MBq.s/kg at imaging time (injected activity corrected for physical decay) and *CV* was obtained according to equation 3. Data available from step 1 were used to cross validate the analytical curve obtained in step 2. Additionally, *CV* values of step 2 were divided into three groups of *CD*: < 200 MBq.s/kg (n=45), 200-300 MBq.s/kg (n=32), 300-400 MBq.s/kg (n=33); and the dispersion of *CV* within groups were verified by computing the *CV* variance ( $\sigma^2_{cv}$ ):

$$\sigma^2_{cv} = \frac{\sum(CV - \overline{CV})^2}{N-1} \text{ (equation 5)}$$

Where  $\overline{CV}$  is the averaged coefficient of variation and *N* is the number of *CV* measurements within a group.

In clinical imaging, *CV* is a function of injected activity, acquisition time, reconstruction, processing, and patient-dependent parameters (eg: body mass). For a particular *CV* and scanner settings, the expected activity and acquisition duration to achieve matched noise levels as a function of object mass is (*adapted from ref. 23*):

$$A.t = \alpha * m^\beta \text{ (equation 6)}$$

Where  $A$  is the injected activity at scan time,  $t$  is the acquisition duration,  $\alpha$  and  $\beta$  are scanner-specific coefficients and  $m$  is the body mass. Previous published data for PSF2 and OSEM3D suggested acquisition parameters that give  $CV = 12\%$  as optimal (24). These acquisition parameters were arranged in equation 6 to benchmark current recommendations, and the results from steps 1 and 2 were used to define  $A.t$  for PSF7.

Figure 2 illustrates the design of the study.

### Statistical analysis

The residuals of regression were tested for normality by using the Shapiro-Wilk test to validate the curve fit of  $CV$  in the liver. An F-test was performed to check for differences between the  $\sigma^2_{cv}$  for group 200-300 MBq.s/kg and the post/previous groups. Graphs and statistical analysis were performed with OriginPro 9.0.0 (OriginLab Corporation, Northampton, MA, USA) and GraphPad Prism 5.01. Where indicated, statistics of  $CV$  were computed following the limits for 95% confidence interval (CI) and  $p < 0.05$  was considered as statistically significant.

## RESULTS

### Phantom Studies

Figure 3 shows the  $CRC_{max}$  curves of each protocol. The EQ.PET filter which harmonizes PSF2 with minimal bias was 6.5 mm (PSF2-EQ6.5), as shown by  $HBI$ s reported in Table 1 and Figure 4, being the  $HBI$  for this reconstruction setting the lowest among the tested EQ.PET filters, thus providing a reasonable low  $HBI$ .

Noise levels in uniform regions are commonly used as an indicator for quantification variability and uniform region noise of  $CV = 15\%$  has been suggested as a limiting noise level (21). Figure 4 demonstrates that  $Q_{var}$  for the PSF reconstructions was lower than OSEM3D for all groups of acquisition parameters (for example, for group C, the noise with PSF is lower than

OSEM3D), leading to less reconstruction-dependent variability. Interpolation of points for OSEM3D in figure 4-A suggests that  $Q_{var} = 4\%$  would be a more reliable limit regardless the reconstruction method. For quantifications with EQ.PET, it is important to stress that EQ.PET performs quantifications only on the spheres (lesions), and the background noise for PSF2 is presented as with 2mm smoothing only in Figure 4.

## **Patient studies**

### **Step 1**

The injected activity and acquisition duration resulted in decay corrected acquisition parameter of  $397 \pm 68$  MBq.s/kg (range: 221-612 MBq.s/kg). The evaluation of background noise in the liver for the step 1 resulted in  $CV = 11.7 \pm 3.6\%$  and  $CV = 6.7 \pm 2.4\%$  (CI = 95%) for reconstructions OSEM3D and PSF7, respectively (Figure 5). Thus, noise in the liver is 1.75 times higher for OSEM3D than for PSF7 ( $p < 0.0001$ ).

### **Step 2**

The plots of liver noise from step 2 (Figure 6) show similar trends as the phantom studies. For a given reconstruction setting, the image noise depends on the activity concentration, acquisition duration, scatter and attenuation conditions, which are similar between the phantom and a 75 kg standard patient due to their similar transaxial section. At scan time, injected activity concentration in patients was similar to phantom (approximately 2 MBq/kg). However, because the SUV is the ratio of local concentration and injected activity concentration, as higher the SUV higher the concentration is relative to the injected activity. Therefore, the liver had two to three times more <sup>18</sup>F-FDG activity (SUV=2-3) than the phantom background (SUV=1). For the liver region, the presence of activity in adjacent volumes penalizes the Noise Equivalent Count Rate (NECR) and negatively impacts image noise. NECR and image noise have different relations according to reconstruction, being images reconstructed with PSF modelling less affected by NECR degradation (22,24). Inhomogeneous <sup>18</sup>F-FDG uptake areas and anatomical noise in the liver is another source of increased noise in

a clinical situation. However, the higher  $^{18}\text{F}$ -FDG activity in the liver dominates over these factors in comparison to phantom.

### **Noise standardization and protocol validation**

By comparing step 1 ( $397 \pm 68$  MBq.s/kg, group B,  $CV = 6.7 \pm 2.4\%$ ,  $CI = 95\%$ ) and step 2 for the same range of  $CD$  ( $388 \pm 36$  MBq.s/kg,  $n = 39$ , body mass =  $73 \pm 18$ ,  $CV = 7.0 \pm 2.4\%$ ,  $CI = 95\%$ ), one can conclude that the two groups have clinically equivalent noise performance. A two-sided t-test was performed to rule out the null hypothesis that the difference in these two groups is greater than 0.7% (indifference zone). As such, we find that the mean difference in the groups was  $0.3 \pm 0.3\%$ , deemed to be equivalent by this definition ( $p < 0.05$ ).

The images of subjects higher than 100 kg (mean:  $113 \pm 12$  kg,  $n = 3$ ,  $CD$ :  $378 \pm 57$  MBq.s/kg) were selected and found  $CV = 7.3 \pm 1.9\%$  ( $CI = 95\%$ ,  $k = 4.3$ ) as predicted by the analytical model where  $CV = 7.2\%$  (Figure 6). These findings support the hypothesis of a linear model for PSF7. Hence, coefficient  $\beta$  in equation 6 may be adjusted to  $\beta = 1$  and  $CD$  in PSF7 may be linearly adjusted according to patient body mass.

Analysis of  $\sigma_{cv}^2$  as a function of  $CD$  showed higher  $\sigma_{cv}^2$  when  $CD < 200$  MBq.s/kg, where  $\sigma_{cv}^2$  were  $3.6 \times 10^{-4}$ ,  $1.4 \times 10^{-4}$  and  $1.6 \times 10^{-4}$  for  $CD < 200$ , 200-300 and 300-400 MBq.s/kg, and mean value of  $CD$  groups were 136.6, 256.2 and 355.4 MBq.s/kg, respectively. F test demonstrated that  $\sigma_{cv}^2$  was statistically different between  $< 200$  and 200-300 MBq.s/kg ( $p = 0.007$ ). However, no significant difference of  $\sigma_{cv}^2$  was observed when 200-300 and 300-400 MBq.s/kg were compared ( $p = 0.69$ ). From this analysis, we can define that  $CD$  higher than 260 MBq.s/kg will provide  $CV$  with acceptable variability for PSF7.

### **Optimal $^{18}\text{F}$ -FDG dose schemes**

Both PSF configurations yielded lower doses as compared to those commonly used in PET studies (Table 2). For optimal PSF2 imaging, 326 MBq.s/kg ( $\beta = 1.48$ ) provides  $CV = 12\%$  in the liver, considered as the “gold standard” (24). The optimal  $CD$  for PSF7 is 260 MBq.s/kg ( $\beta = 1$ ) which will result in 106, 158 and 211 MBq injected activity for respectively 50, 75 and

100 kg body masses. Thus, PSF could guide the design of new low dose PET protocols in the range 260-326 MBq.s/kg for a 75 kg standard patient, and  $\beta$  between 1-1.5.

Figure 7 shows the injected activity for each reconstruction protocol. Ideally, lesion detectability should be maximized by using PSF with minimum filtering (9) while maintaining SUV harmonization (EQ.PET) and injected activity as low as possible. On the other hand, detectability relies on a tradeoff among injected activity and reconstruction preferences (8). Therefore, PSF7 would provide the lowest injected activity and image quality still within international standards.

## **DISCUSSION**

This study aimed to derive optimal 18F-FDG PET/CT imaging protocols as a function of body mass to achieve quantification consistent with the EARL criteria while keeping the image noise standardized. The use of harmonized metrics may help with personalized medicine since these enable more reliable assessment of tumor characteristics. Advances in hardware and image reconstruction PET technology can allow for decreased 18F-FDG injected activity but the exact influence of PSF for 18F-FDG dose optimization and harmonized quantification is still unclear.

### **EARL harmonization and patient-specific dose schemes**

Overall compliance rate of EARL applicants due to *CRC* inconsistencies is reported as only 63% (14). Other authors have published data with EARL quantification slightly outside the EARL limits (14,28,33), but they did not state the magnitude of bias. In this work we defined a harmonization bias index (*HBI*) to quantify agreement with the EARL standards. It is important to note that the *HBI* metric has limitations to objectively compare different bias configurations. For example, multiple spheres could be slightly biased and have the same *HBI* of a configuration which one sphere is very biased; also, *HBI* does not tell the direction of bias (eg.: if

recovery coefficients are too low or too high). However, the proposed metric is useful to address the magnitude of the “slightly bias” frequently reported in the literature.

For patient studies, which patient habitus strongly affects the (NECR) curves, higher injected activity will result in loss of data quality that influences image quality. Therefore, increasing the acquisition duration is more effective than increasing the injected activity to preserve the image quality (25). That is,  $\beta$  value depends on the acquisition duration and the injected activity, and  $\beta$  will be smaller if the injected activity is limited to smaller values. In our facility, the injected activity for larger patients (>90kg) is limited to 3 MBq/kg and the acquisition duration is adjusted accordingly to maintain the counting statistics.

### **Reconstruction-specific dose schemes**

We showed that reconstructing the same raw data with PSF2 yielded an acquisition parameter that was more linear as a function of mass than OSEM3D (24). In other words, the PSF2 reconstruction had a lower  $\beta$  value in the PSF reconstruction (equation 6). Thus, the optimal acquisition parameter for noise standardization should be adjusted according to patient-specific parameters (ex: body mass) by using reconstruction-specific power equations, contrary to the generalized quadratic method (21, 23).

In this work, we used 164 datasets (4 images per patient) to obtain the noise curve with count levels that mimic a clinical situation. Differences between coefficient  $b$  (equation 2) as compared with Figure 4 could be attributed to the fact that patient mass may not be sufficient to normalize across very different morphologies. However, the residuals of regression were normally distributed in the Shapiro-Wilk test of normality ( $w=0.359$ ,  $p<0.05$ ).

We compared the performance of regular OSEM3D and low dose PSF configurations regarding the EARL compliance,  $SUV_{max}$  variability ( $Q_{var}$ ), and CV variance ( $\sigma^2_{cv}$ ) in the liver. Our results showed that a linear approach is feasible for PSF7 with 260 MBq.s/kg which performs similarly to OSEM3D with 400 MBq.s/kg. However, the small cohort of patients

greater than 100 kg (n=3) was a limitation in our study, encouraging its future validation on a larger population.

We demonstrated that strong filtering (PSF2-EQ6.5 and PSF7) improved the SUV variability of PSF over OSEM3D for same counting level. This is especially important for monitoring of a disease or designing new protocols when low dose is required like the recently interest for screening with PET.

### **Final considerations**

Clinical SUV measurements are prone to numerous sources of error related to technical, physical and biological factors (34-37). While the EANM guideline recommends following strict technical factors (cross calibration, clocks synchronization, etc), the physical related factors (acquisition and reconstruction parameters) mirrored in the *CRC* values are quite wide and differences between the minimum and maximum EARL limits are within 20-45% from the largest to the smallest spheres (12-14), showing that one must still be cautious when quantifying lesions with different protocols.

In the context of EARL accreditation, it is challenging that a large pool of imaging systems to converge to the “same” *CRC* curve (14). The implementation of PSF reconstruction with narrow gaussian filtering amplitudes allows that the smaller spheres of NEMA phantom to reach higher *CRC* values, but the Gibbs effects overshoots quantification of the 17 mm sphere (38). This was resolved with strong gaussian filtering and, consequently, the *CRCs* of 10mm and 13mm spheres were very close to the lower *CRC* limits. The EQ.PET filter, however, may be easily setup with narrower filter while quantifying smaller lesions (<13mm) in the same reconstructed image.

Of course, EARL limits are not ideal, but feasible recommendations for most PET scanner generations to achieve minimal standards. On the other hand, alternatives of reconstruction configurations are encouraged as to match the *CRC* with minimal differences (34).

This work did not directly assess the relationship of acquisition and reconstruction parameters and detectability. Ideally, we would find protocols that achieve a sufficient level of quantification and detectability performance. We fall short of this goal using quantification and background noise as a surrogate for detectability under the assumption that this is reflective of contrast to noise, a metric correlated with detectability. While this is a limitation, our work represents one of the few studies attempting to find protocols with appropriate quantification and background noise levels.

Acquisition parameter adjustments accordingly to patient habitus and reconstructions are required to maintain the image noise standardized through patients' population and ensure consistent image quality and quantifications. Our method to achieve low dose PSF based protocols will also allow for management improvements of PET facility by scanning the patients faster and/or decreasing the patient dosimetry and the radiopharmaceutical costs.

## **CONCLUSIONS**

This study provides scanner and patient-specific recommendations for optimized oncological <sup>18</sup>F-FDG PET/CT imaging protocol when PSF modelling reconstruction is applied aimed at obtaining compliance with the EARL standards. Optimal PET acquisition and reconstruction settings will allow for a) reduction of scan's duration or administered <sup>18</sup>F-FDG activity, and b) consistent assessment of metabolic tumor activity, aligned with demands for personalization of patient assistance.

## **ACKNOWLEDGMENTS**

We thank the Comissao Nacional de Energia Nuclear (CNEN, Brazil) and the International Atomic Energy Agency (IAEA) for the efforts to develop the nuclear medicine at our institutions through a Technical Cooperation project. We also thank both reviewers for the crucial comments which improved the quality of our work.



No potential conflict of interest relevant to this paper is reported. All data collected and presented in this paper were derived from human patients, after signing official consent and participation forms.

#### **CONFLICT OF INTEREST**

The authors declare no conflict of interest.

## REFERENCES

1. Ambrosini V, Nicolini S, Caroli P, et al. PET/CT imaging in different types of lung cancer: an overview. *Eur J Radiol.* 2012;81:988-1001.
2. Weber WA. Use of PET for monitoring cancer therapy and for predicting outcome. *J Nucl Med.* 2005;46:983–95.
3. de Geus-Oei LF, van der Heijden HF, Corstens FH, Oyen WJG. Predictive and prognostic value of FDG-PET in nonsmall-cell lung cancer: a systematic review. *Cancer.* 2007;110:1654–64.
4. Boellaard R. The engagement of FDG PET/CT image quality and harmonized quantification: from competitive to complementary. *Eur J Nucl Med Mol Imaging.* 2016;43:1-4.
5. Boellaard R. Optimisation and harmonisation: two sides of the same coin? *Eur J Nucl Med Mol Imaging.* 2013;40:982-984.
6. Andersen FL, Klausen TL, Loft A, Beyer T, Holm S. Clinical evaluation of PET image reconstruction using a spatial resolution model. *Eur J Radiol.* 2013;82:862-869.
7. Schaefferkoetter J, Casey M, Townsend D, Fakhri G. Clinical impact of time-of-flight and point response modeling in PET reconstructions: a lesion detection study. *Phys Med Biol.* 2013;58:1465.
8. Adler S, Seidel J, Choyke P, et al. R. Minimum lesion detectability as a measure of PET system performance. *EJNMMI physics.* 2017;4:13.
9. Kadrmas DJ, Casey ME, Conti M, Jakoby BW, Lois C, Townsend DW. Impact of time-of-flight on PET tumor detection. *J Nucl Med.* 2009;50:1315-1323.
10. Tong S, Alessio AM, Kinahan PE. Noise and signal properties in PSF-based fully 3D PET image reconstruction: an experimental evaluation. *Phys Med Biol.* 2010;55:1453.
11. Rahmim A, Qi J, Sossi V. Resolution modeling in PET imaging: theory, practice, benefits, and pitfalls. *Med Phys.* 2013;40.

12. New EANM FDG PET/CT accreditation specifications for SUV recovery coefficients. EANM research Ltd (EARL) website. [http://earl.eanm.org/cms/website.php?id=/en/projects/fdg\\_pet\\_ct\\_accreditation/accreditation\\_specifications.htm](http://earl.eanm.org/cms/website.php?id=/en/projects/fdg_pet_ct_accreditation/accreditation_specifications.htm). Updated Jan 30, 2017. Accessed Dec 30, 2017.
13. Boellaard R, Hristova I, Ettinger S, et al. EARL FDG-PET/CT accreditation program: Feasibility, overview and results of first 55 successfully accredited sites. *J Nucl Med*. 2013;54(suppl 2):2052.
14. Kaalep A, Sera T, Oyen W, et al. EANM/EARL FDG-PET/CT accreditation - summary results from the first 200 accredited imaging systems. *Eur J Nucl Med Mol Imaging*. 2018; 45:412.
15. Schaefferkoetter J, Townsend DW. Quantitative Accuracy and Lesion Detectability of Low-Dose FDG-PET for Lung Cancer Screening. *J Nucl Med*. 2016;58:399-405.
16. Lodge MA, Chaudry MA, Wahl RL. Noise considerations for PET quantification using maximum and peak standardized uptake value. *J Nucl Med*. 2012;53:1041-1047.
17. Akamatsu G, Ikari Y, Nishida H. Influence of statistical fluctuation on reproducibility and accuracy of  $SUV_{max}$  and  $SUV_{peak}$ : a phantom study. *J Nucl Med technol*. 2015;43:222-226.
18. Schmidlein C, Beattie BJ, Bailey DL, et al. Using an external gating signal to estimate noise in PET with an emphasis on tracer avid tumors. *Phys Med Biol*. 2010;55:6299.
19. Armstrong IS, Kelly MD, Williams HA, Mattheus JC. Impact of point spread function modelling and time-of-flight on FDG uptake measurements in lung lesions using alternative filtering strategies. *EJNMMI Physics*. 2014;1:99.
20. Boellaard R, Delgado-Bolton R, Oyen WJ, et al. FDG PET/CT: EANM procedure guidelines for tumour imaging: Version 2.0. *Eur J Nucl Med Mol Imaging*. 2015;42:328–354.
21. Koopeman D, van Osch JA, Jager PL, et al. Technical note: how to determine the FDG activity for tumor PET imaging that satisfies European guidelines. *Eur J Nucl Med Mol Imaging Phys*. 2016;3:22.

22. Akamatsu G, Ishikawa K, Mitsumoto K, et al. Improvement in PET/CT image quality with a combination of point-spread function and time-of-flight in relation to reconstruction parameters. *J Nucl Med*. 2012;53:1716-1722.
23. de Groot EH, Post N, Boellaard R, Wagenaar NRL, Willemsen ATM, Dalen JA. Optimized dose regimen for whole-body FDG-PET imaging. *Eur J Nucl Med Mol Imaging*. 2013;3:63.
24. Menezes VO, Machado MAD, Queiroz CC, et al. Optimization of oncological 18F-FDG PET/CT imaging based on a multiparameter analysis. *Med Phys*. 2016;43:930-938.
25. Wickham F, McMeekin H, Burniston M, et al. Patient-specific optimisation of administered activity and acquisition times for 18 F-FDG PET imaging. *EJNMMI research*. 2017;7:3.
26. Spadafora M, Pace L, Mansi L. Segmental 18F-FDG-PET/CT in a single pulmonary nodule: a better cost/effectiveness strategy. *Eur J Nucl Med Mol Imaging*. 2016.
27. Veronesi G, Bellomi M, Veronesi U, et al. Role of positron emission tomography scanning in the management of lung nodules detected at baseline computed tomography screening. *Ann Thorac Surg*. 2007;84:959-966.
28. Lasnon C, Desmots C, Quak E. Harmonizing SUVs in multicentre trials when using different generation PET systems: prospective validation in non-small cell lung cancer patients. *Eur J Nucl Med Mol Imaging*. 2013;40:985-996.
29. Quak E, Roux P, Hofman M. Harmonizing FDG PET quantification while maintaining optimal lesion detection: prospective multicentre validation in 517 oncology patients. *Eur J Nucl Med Mol Imaging*. 2015;42:2072-2082.
30. Lasnon C, Salomon T, Desmots C, et al. Generating harmonized SUV within the EANM EARL accreditation program: software approach versus EARL-compliant reconstruction. *Ann Nucl Med*. 2017;31:125-134.
31. EARL procedure for assessing PET/CT system specific patient FDG activity preparations for quantitative FDG PET/CT studies. EANM research Ltd (EARL) website.

[http://earl.eanm.org/html/img/pool/EARL-procedure-for-optimizing-FDG-activity-for-quantitative-FDG-PETstudies\\_version\\_1\\_1.pdf](http://earl.eanm.org/html/img/pool/EARL-procedure-for-optimizing-FDG-activity-for-quantitative-FDG-PETstudies_version_1_1.pdf). Updated Jan 30, 2017. Accessed Mar 27, 2017.

32. Wahl RL, Jacene H, Kasamon Y, Lodge MA. From RECIST to PERCIST: evolving considerations for PET response criteria in solid tumors. *J Nucl Med*. 2012;50(Suppl 1):122S-150S.
33. Ptacek J, Karhan P, Fiala P. Optimal reconstruction matrix and PET image filtration for point-spread function and time-of-flight reconstruction – A phantom study. *Phys Med*. 2017;39:95-99.
34. Lodge MA. Repeatability of Standardized Uptake Value in Oncologic 18F-FDG PET. *J Nucl Med*. 2017;58:523-532.
35. Boellaard R. Standards for PET image acquisition and quantitative data analysis. *J Nucl Med*. 2009;50(Suppl 1):11S-20S.
36. Aide N, Lasnon C, Veit-Haibach P, Sera T, Sattler B, Boellaard R. EANM/EARL harmonization strategies in PET quantification: from daily practice to multicentre oncological studies. *Eur J Nucl Med Mol Imaging*. 2017;1-15.
37. Adams MC, Turkington TG, Wilson JM, Wong TZ. A systematic review of the factors affecting accuracy of SUV measurements. *Am J Roentgenol*. 2010; 195:310-320.
38. Munk OL, Tolbod LP, Hansen SB, Bogsrud TV. Point-spread function reconstructed PET images of sub-centimeter lesions are not quantitative. *EJNMMI physics*. 2017;4:5.

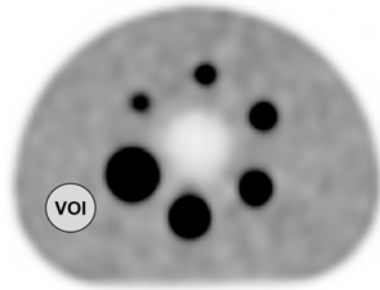


**FIGURE 1.** Positioning of 3 cm diameter VOI for CV calculation.

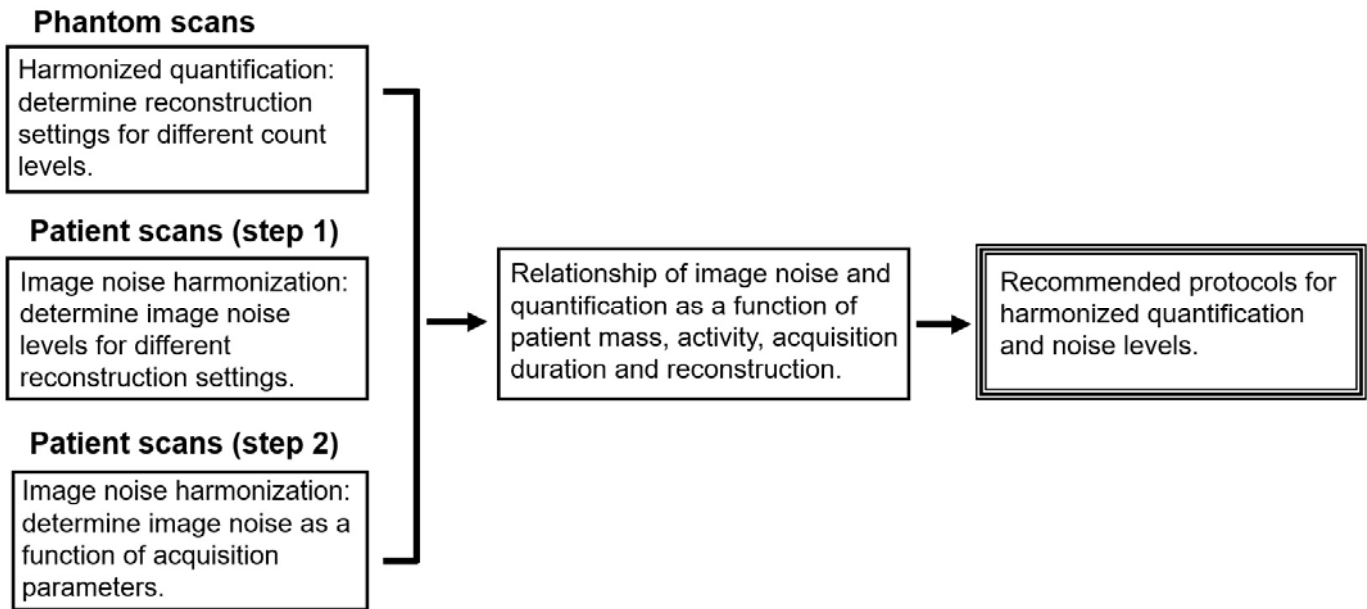


**FIGURE 2.** Flow chart to achieve low dose and task specific protocols.

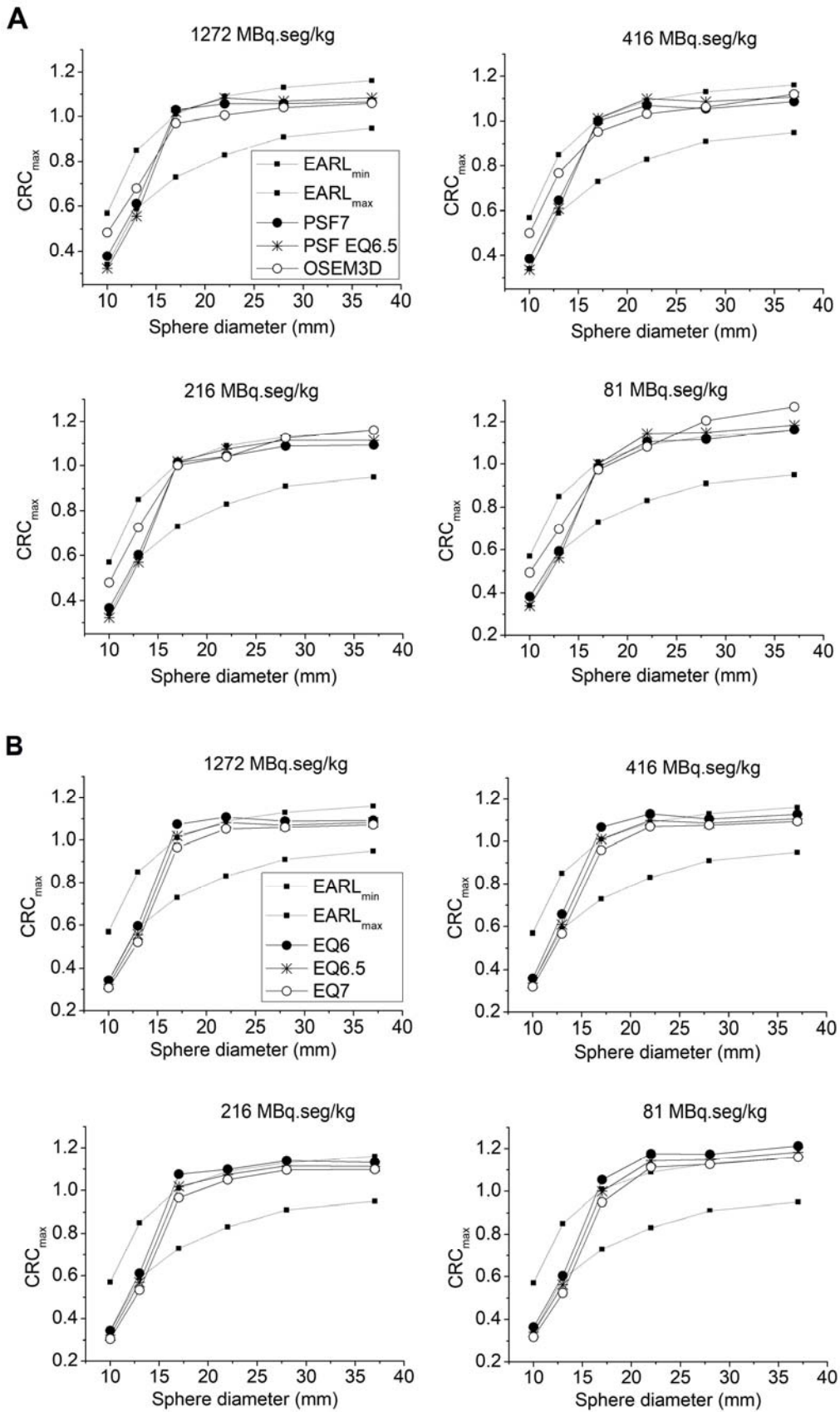
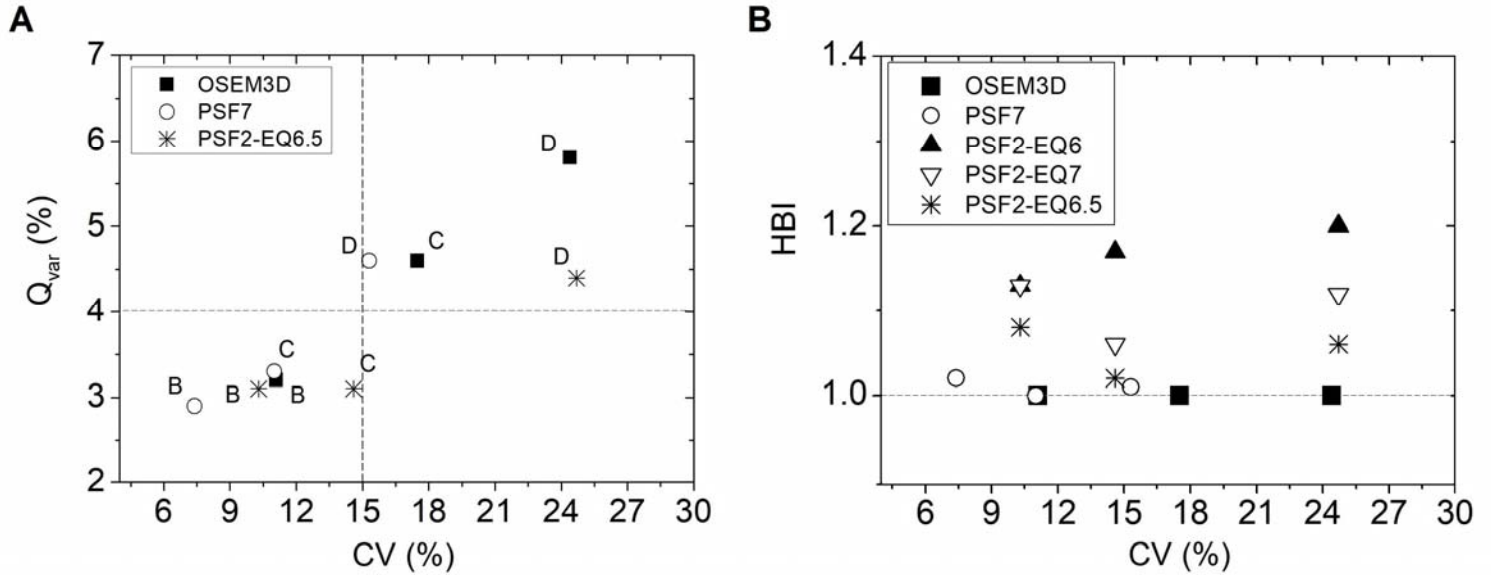
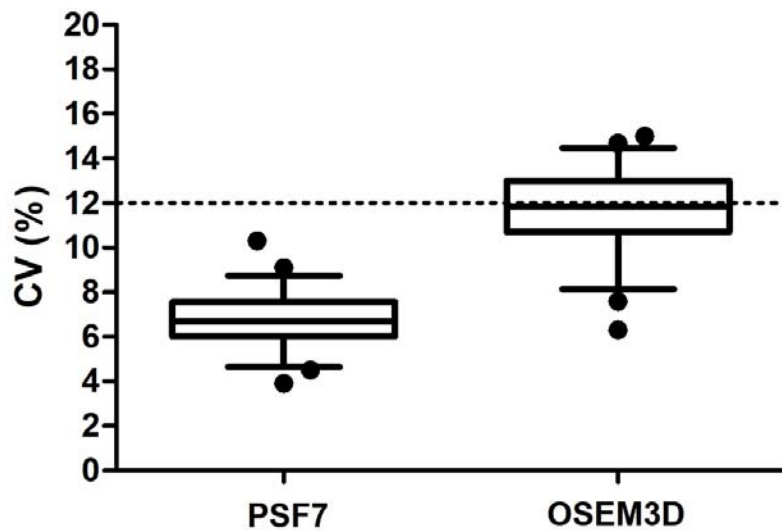


FIGURE 3.  $CRC_{max}$  for OSEM3D, PSF7 and PSF2-EQ\* protocols.



**FIGURE 4.** Quantification variability (A) and harmonization bias index (B) versus image noise. Plots represent CV generated from acquisitions of group B, C and D. Dashed lines represent the limits of acceptability for  $Q_{var}$  (A) and  $HBI$  (B), where  $CV = 15\%$  is the EARL reference.



**FIGURE 5.** Comparison of CV between PSF7 and OSEM3D. Dashed line means OSEM3D and PSF2 noise obtained from formulations in ref. 24.



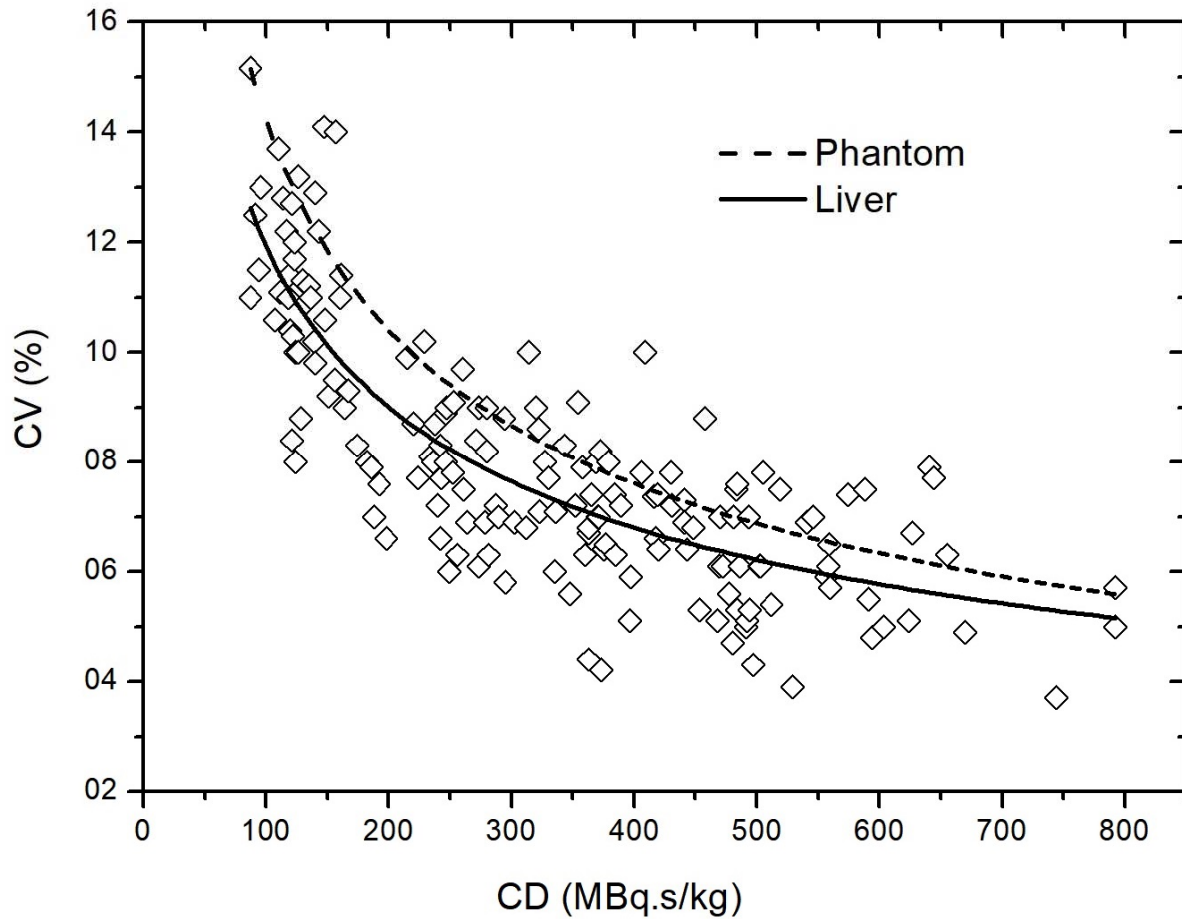


**FIGURE 6.** Plot of uniform region, liver noise (*CV*) versus acquisition parameter for patient data from step 2 using PSF7. The curve fit to this liver data (solid line) and to the phantom data (dashed line) were generated with fitting coefficients  $a=0.77$ ,  $b=-0.40$ ,  $R^2=0.67$ ; and  $a=1.40$ ,  $b=-0.49$ ,  $R^2=0.98$  for liver and phantom, respectively.

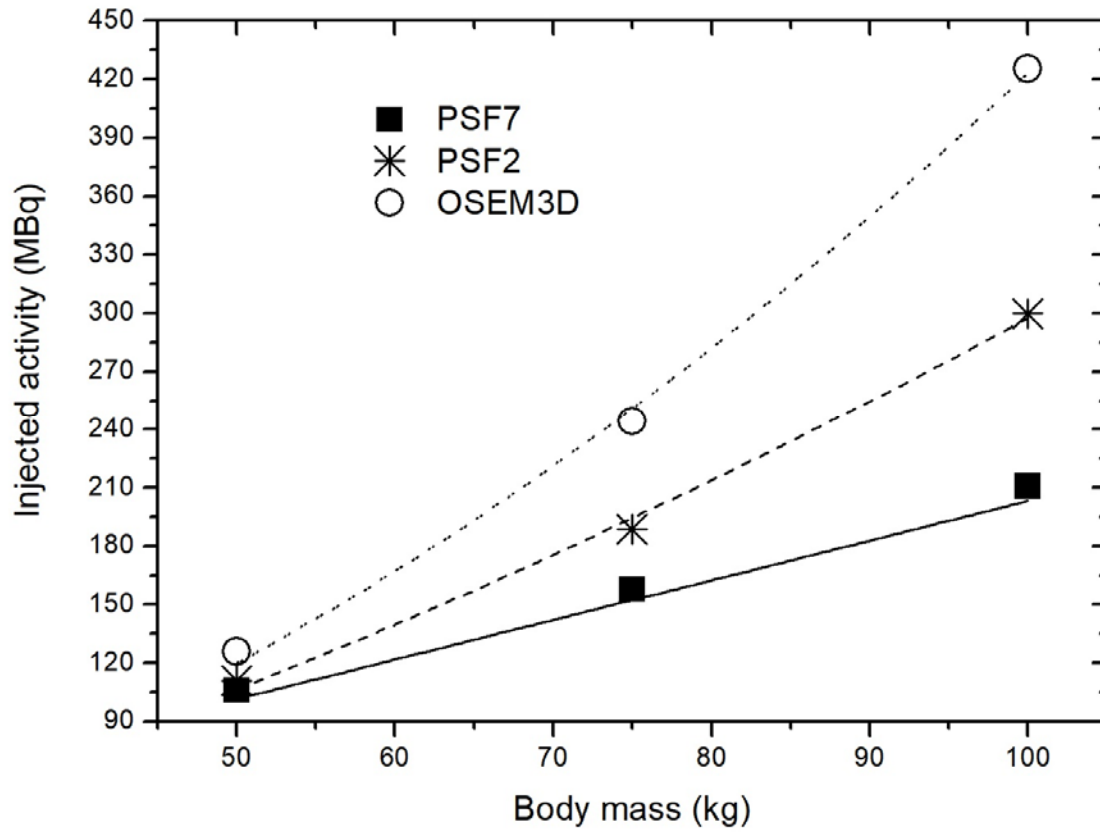


**FIGURE 7.** Dose scheme illustration. Injected activity for 60 min uptake time and normalized to 3 min duration per bed acquisition.

**TABLE 1.** Harmonization bias indexes for groups of acquisition parameters and different reconstruction settings

Acquisition parameter		<i>HBI</i>				
		OSEM3D	PSF7	PSF2-EQ6	PSF2-EQ6.5	PSF2-EQ7
Group A	1272 MBq.s/kg	1.00	1.02	1.13	1.08	1.13
Group B	416 MBq.s/kg	1.00	1.00	1.17	1.02	1.06
Group C	216 MBq.s/kg	1.00	1.01	1.20	1.06	1.12
Group D	81 MBq.s/kg	1.29	1.02	1.40	1.18	1.15

**TABLE 2.** Optimal counting levels at scan time and derived 18F-FDG injected activity.

	<b>Equation</b>	<b>Injected Activity (MBq)</b>		
	<b><math>A.t</math> (MBq.s)</b>	<b>50 kg</b>	<b>75 kg</b>	<b>100 kg</b>
<b>PSF7</b>	$A.t = 260 * m$	106	158	211
<b>PSF2 (24)</b>	$A.t = 41 * m^{1.48}$	111	189	300
<b>OSEM3D (24)</b>	$A.t = 12 * m^{1.82}$	126	244	426

A: activity at scan time,  $t$ : acquisition duration,  $m$ : body mass. Coefficients  $\alpha$  and  $\beta$  (equation 7) for OSEM3D and PSF2 were determined through regression of data from table V in ref. 24. Injected activity is decay corrected for 60 minutes prior to scan time and typical 3 minutes acquisition duration per bed position.